

RESEARCH ARTICLE

Evaluation and improvement of shear-strength expressions for circular concrete-filled steel tubes

Mu-Zi Zhao¹, Dawn E. Lehman^{2*}, Xin Zhang³, Charles W. Roeder²

- ¹ Central Research Institute of Building and Construction (Shenzhen) Co., Ltd., MCC Group, Shenzhen, China
- ² University of Washington, Seattle, WA, United States
- ³ Yanshan University, Qinhuangdao City, Hebei Province, China

Article History

Received 17 November 2022 Accepted 3 July 2023

Keywords

Concrete-filled steel tube (CFST) Shear behavior Contribution of steel Contribution of concrete

Abstract

The accuracy of the shear resistance design equation for concrete-filled steel tubes (CFSTs) is crucial to ensure the safety of CFST structures. However, the current design equations underestimate the test data, and cannot accurately predict the relative shear resistance of the steel and concrete fill. To solve this problem, this paper developed an advanced finite element model in the LS-Dyna program, which was validated using experimental results of CFST members failing in shear. A systematic parametric study was then conducted. The result showed that the contribution of the steel increased significantly with the strain-hardening ratio (F_u/F_y) while the contribution of concrete fill was greatly influenced by the internally reinforced ratio (ρ_{int}) and axial load level (P/P_0) . These predictions were combined with the experimental results to develop a more accurate and reliable design expression for the shear strength of circular CFSTs.

1. Introduction

Concrete-filled steel tubes (CFSTs) are structurally robust members [1,2]. CFSTs are strong in combined axial load and bending, so CFST components are commonly used for deep piles and drilled shaft foundations [3,4]. The efficiency and strength of circular CFST are a result of the optimum placement of the steel tube to resist bending and the use of the infill concrete to resist high-compression loads. The concrete fill also stiffens the steel tube to prevent premature local tube buckling, and the tube provides confinement to the concrete fill. CFSTs accelerate construction because formwork, shoring, and internal reinforcing bar cages (except within the connection region for some connections) are not needed. Further, the steel tube supports loads during construction and curing of concrete fill and there is no need to delay construction until a specific concrete strength is achieved.

In the US, there is a preference for circular CFSTs in bridge systems [5], although rectangular CFSTs are used for building construction. This paper addresses circular CFSTs since they are more commonly used and tested.

eISSN 2630-5763 © 2023 Authors. Publishing services by golden light publishing®.

^{*} Corresponding author (delehman@uw.edu)

For a given load, a circular CFST requires a smaller diameter than a reinforced concrete (RC) component with the same strength. While the combined flexural and axial behavior is well studied and understood, the shear strength of circular CFSTs has received less attention in the literature. As such, the shear resistance of circular CFSTs is not as well understood. This is rational since the shear demands on typical CFST columns and piles are not large. However, lateral spreading or seismically induced liquefaction of soil layers can induce very large shear forces in the deep pile or drilled shaft foundations. It is necessary to understand the shear-dominated behavior of CFST and have design equations that reliably predict their shear resistance.

Experimental studies on circular CFSTs subjected to shear loading have been conducted in China (e.g., [68]), Japan (e.g., [9]) and the US (e.g., [10,11]). These investigations cover important design parameters including (1) the compressive concrete strength, (2) the yield strength of steel (F_y), (3) the shear span-to-diameter ratio (a/D), (4) the diameter of the CFST (D), (5) the axial load ratio (P/P_0), (6) the internal reinforcement ratio (ρ_{int}), and (7) the bond condition between steel tube and concrete. The collective findings from these investigations are: (1) shear failure does not occur for a/D greater than 0.5 [6,8], (2) the shear strength increased with an increase in the P/P_0 ratio [8,10], (3) composite action between the steel tube and infill concrete is needed to develop the full shear resistance [10], and (4) internal reinforcement has a much smaller contribution to the total shear capacity and in many cases can be neglected [10].

In addition to the experimental research, two significant finite element analysis (FEA) studies were also conducted: Lehman et al. [12] and Kenarangi and Bruneau [11], which are summarized here to compare their approaches, limitations, and findings.

Lehman et al. [12] used the ABAQUS computer program and the concrete damage plasticity model (CDPM) available in that program to both study the experiments and conduct a parametric study to further the testing program. The analyses accurately predicted the elastic behavior obtained in experiments but peak shear resistance, inelastic deformation, and damage to the concrete fill were underestimated in some. These inaccuracies resulted from inaccuracies in the concrete model used; however, it was one of the best models available at the time of that study. The results of the parametric study and available test data were combined to propose a shear-strength equation in the form of a two-contribution model. The authors used the total strength rather than separating the shear contributions of the steel tube and concrete fill because of the limitations of the concrete constitutive model. There was more certainty in the contribution of the steel tube to the total shear strength, and, as such, the contribution of the infill concrete to the shear strength was determined indirectly, by removing the contribution of the steel tube, V_{st} , from the total shear strength, V_n .

The other significant combined experimental and FEA study was conducted by Kenarangi and Bruneau [12]. This research team took a different approach in that (1) LS-Dyna was used with the Winfrith concrete model and (2) the two components were determined from the analysis results for one of the specimens. Because a parametric study was not conducted, the proposed design equation was based on this simulation. Prior work [13] demonstrates that the Winfrith model cannot capture the deterioration of the concrete compressive strength, which can lead to an overestimation of the concrete contribution and an underestimate of the steel tube contribution to the shear strength. As such, both studies, although advanced in their approaches, failed to fully simulate the strength and degradation of CFST failing in shear.

This research study was undertaken to use a more accurate finite-element modeling approach to extend the existing database to evaluate and improve current design equations. The research was conducted in four phases. First, the current equations were evaluated using an experimental database. Second, an advanced modeling approach was used, including a new concrete constitutive model and a new bond model available in LS-Dyna; this model was validated using prior experimental results of circular CFSTs [13]. The third phase of the study used to model to conduct a parametric study. The results of each analysis model were used to determine the separate components of the shear strength, specifically the individual contributions of the steel tube and concrete fill following the approach developed by Kenarangi and Bruneau [12]. The last phase

used the simulation results and prior test results to evaluate the codified equations and provide a basis for a more accurate design model.

2. Codified shear-strength design equations

The shear capacity of a CFST is larger than a tube alone because (1) tube buckling restraint by concrete fill, which allows yielding of the full cross-section and increases the post-yield capacity of steel tube [10] and (2) confinement effect on concrete fill by the tube which increases the shear strength of the concrete fill [8,10]. However, most codified design expressions depend on the shear strength of the steel tube alone. As a result, design expressions are prone to underestimating the shear resistance of circular CFSTs.

Eqs. (1)-(8) present codified design equations in the US [14,15], Europe [16], and China [17]. In contrast, the approach in concrete design is to include the contribution of the steel and the concrete; this approach has been adopted by AISC 360-22 [14]. The equations use the variables provided in the code itself. Note that these variables are all defined in the notation list.

AISC 360 (2022)
$$V_{n(AISC 360)} = 0.6(0.5A_s)F_y + 0.06K_cA_c\sqrt{f_c'}$$
 (1)

AASHTO
$$V_{n(\text{\tiny AASHTO})} = 0.498\sqrt{f_c'}A_c + \frac{2Dt}{\sqrt{3}}F_y \tag{2}$$

Eurocode
$$V_{n(\text{EC4})} = \frac{2A_s}{\pi} \left(F_y / \sqrt{3} \right) \tag{3}$$

Chinese code 1
$$V_{n_{\text{(Chinal)}}} = 0.71 f_{sv} A_{sc}$$
 (4)

$$f_{sv} = 1.547 F_{y} \frac{\alpha_{sc}}{\alpha_{sc} + 1}$$
 (5)

Chinese code 2
$$V_{n(\text{China2})} = (V_0 + 0.1P) \left(1 - 0.45\sqrt{\frac{a}{D}}\right)$$
 (6)

$$V_0 = 0.2A_c f_c (1 + 3\xi) \tag{7}$$

$$\xi = \frac{A_s F_y}{A_c f_c'} \tag{8}$$

The equations in US codes (AISC 360 and AASHTO) are provided in Eqs. (1) and (2) [14,15]. Both equations use a two-component shear-strength model. The shear-strength equation in the Eurocode is provided in Eq. (3), as $V_{n(\text{Ecd})}$ [16]. This equation includes only the shear strength of the steel tube. Eqs. (4) and (6) provide two different equations for shear strength that are in the Chinese code, $V_{n(\text{Chinal})}$ and $V_{n(\text{Chinal})}$ [17], where Eq. (4) is based on torsion analysis for circular CFST and Eq. (7) is based on research by Xiao et al. [6]. Eq. (4) accounts for only the shear strength provided by the steel tube. Eq. (6) provides the shear strength as a function of the axial load, aspect ratio, as well as concrete-fill and steel-tube properties.

Table 1. Evaluation of code equations

Codes	des AISC [14]		Eurocode [16]	Chinese code-1 [17]	Chinese code-2 [17]	
Average value	2.23	2.06	2.56	0.86	1.48	
COV	0.37	0.31	0.32	0.32	0.30	

A previously compiled test database [6–11, 18] was used to evaluate current code expressions. Table 1 shows the average and coefficient of variation (COV) for the measured to predicted strength ratio for each code. The US and Eurocode expressions provide a very conservative estimate of the strength, where the measured strength is more than twice the predicted. In contrast, the Chinese code-1 [17] overestimates the shear resistances and thus is deemed unsafe; this is likely due to the use of the full area. This suggests that none of these equations are appropriate for load and resistance design approaches.

3. Finite element modeling approach

The finite element modeling approach is based on the work by Zhao et al. [13]. To validate the model, the tests conducted by Lehman et. al. [10] were modeled. These tests were selected because they used large-diameter (508 mm) tubes, investigated many parameters, the test data was readily available and the damage states of the steel tube and the concrete after testing were available.

The test subjected a CFST specimen to shear and moment demands using a four-point bending loading configuration, shown in Fig. 1. There are three distinct regions of interest: (1) the constant moment region, (2) the shear region, and (3) the length of the CFST beyond the support referred to as "the tail length". This tail length is needed to develop full shear stress transfer, i.e., composite action, between the concrete fill and the steel tube.

The finite element model (FEM) of the specimen has five primary components: the steel tube, the concrete fill, the internal reinforcement, the bond between the tube and the concrete fill, and the bond between the internal reinforcement and the concrete fill. To ensure the boundary conditions were accurate, the support cradle and the load cradle were also modeled. Fig. 2 shows the modeling approach. To ensure contact between the load and support cradles and the specimen, a cotton duck-bearing pad was placed between the specimen and the cradle. This was also modeled, as indicated in Fig. 2.

The following highlights the important aspects of the model.

- The steel tube was modeled using Belytschko-Tsay four-node shell elements with two integration points through the thickness.
- The support cradle, internal reinforcement when used, and the cotton duck bearing pads, which
 soften the hard contact at load points of CFST, were modeled as truss elements (ELFORM = 3 in
 LS-Dyna) with MAT003 bilinear kinematic plasticity material behavior (MAT_003 is the material
 designation used in LS-Dyna).
- The load cradle was modeled with 3-dimensional, constant stress, solid elements. These elements used a steel elastic modulus (E_s) of 210,000 MPa and Poisson's ratio of 0.3.

The primary difference and advancement in this modeling approach relative to the prior is the use of a new concrete damage plasticity model (CDPM). This CDPM is capable of simulating damage and deterioration to the concrete fill resulting from compression and tension under both monotonic and cyclic loading [19]. This prior research also indicates that other concrete constitutive models do not have the accuracy of the CDP model implemented in LS-Dyna.

The concrete was modeled with eight-node, constant stress, solid elements (ELFORM=1 in LS-Dyna) with MAT_273 Concrete Damage Plasticity model (CDP) model [20,21]. The elastic modulus (E_c) of the concrete was 34,000 MPa (measured E_c was adopted in validation) and Poisson's ratio was 0.2.

A mesh refinement study was performed to determine the mesh size which would provide accuracy and efficiency in the solution [12]. The final mesh size of the steel tube and outside surface of the concrete fill was 25.4 mm in the shear and constant-moment regions. A mesh size of 50.8 mm was used in the overhang beyond the support, as shown in Fig. 2. The load cradles had a mesh size of 25.4 mm to match the steel tube. The aspect ratio of each element was 1.5 or less.

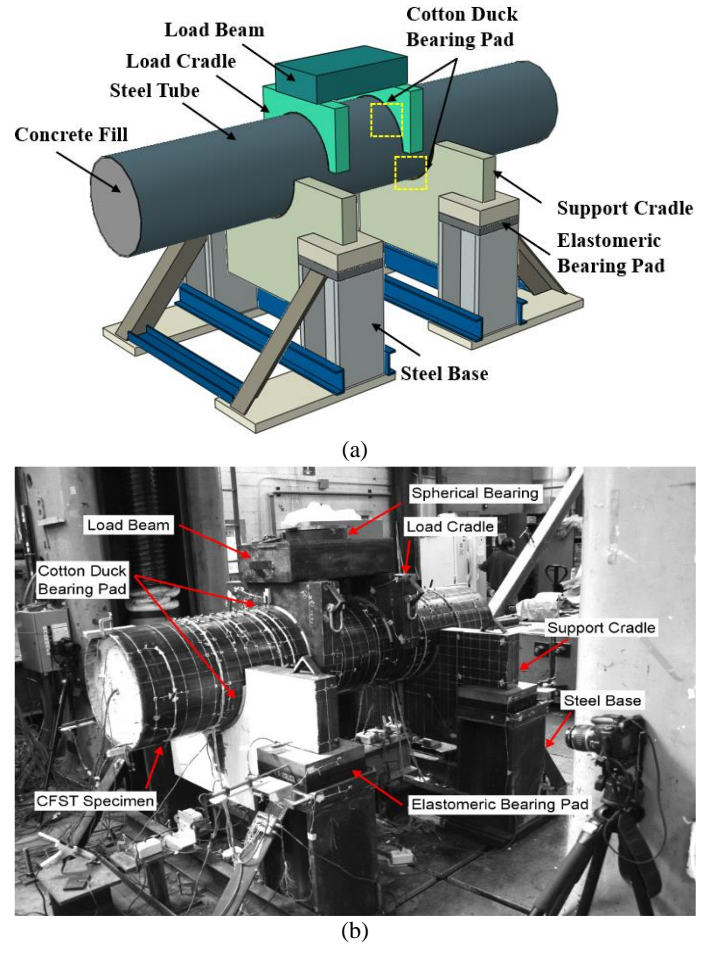


Fig. 1. Test setup with the specimen in space: (a) Schematic and (b) Photograph [10]

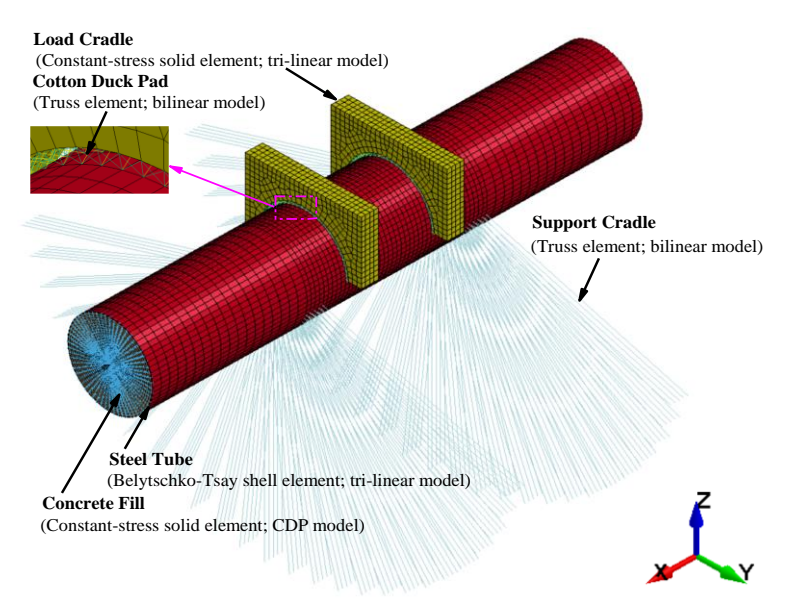


Fig. 2. FE model in LS-Dyna

Compressive damage is controlled by an exponential stress-inelastic strain law shown in Fig. 3a. The compressive damage parameter ε_{fc} , shown in Fig. 3a, controls the strain-softening behavior in compression, which is illustrated by the intersection between the tangential line (dashed line) of the compressive post-peak curve and the x-axis. The value of ε_{fc} was set at 0.0008.

A bi-linear stress-inelastic displacement law was used to quantify the tensile damage behavior of concrete fill, as shown in Fig. 3b. Within LS-Dyna, TYPE = 1 (bilinear softening) was chosen for the tensile damage type of the CDP model. The tensile threshold value, w_f , for linear damage formulation was calculated using Eq. (9) [19]

$$w_f = 4.444G_f/f_t (9)$$

where f_t is the uniaxial tensile strength and G_f (N/m) is the fracture energy of concrete. G_f is calculated using Eq. (10). Additional information about the compressive and tensile damage models can be found in the reference paper [21].

$$G_f = 73(f_c')^{0.18} (10)$$

Fig. 4 illustrates the material properties of the steel used in these analyses. The yield stress, F_y , the corresponding yield strain, ε_y , and the ultimate stress, F_y , for the steel tube. (Note that the values used for the validation study are provided in Table 2) The end of the yield plateau was set to be $10\varepsilon_y$. The tangent modulus in the strain-hardening phase (E_{sh}) was $0.01E_s$. The values of the strains at ultimate stress (ε_0) and fracture (ε_u) are 0.1 and 0.22, respectively.

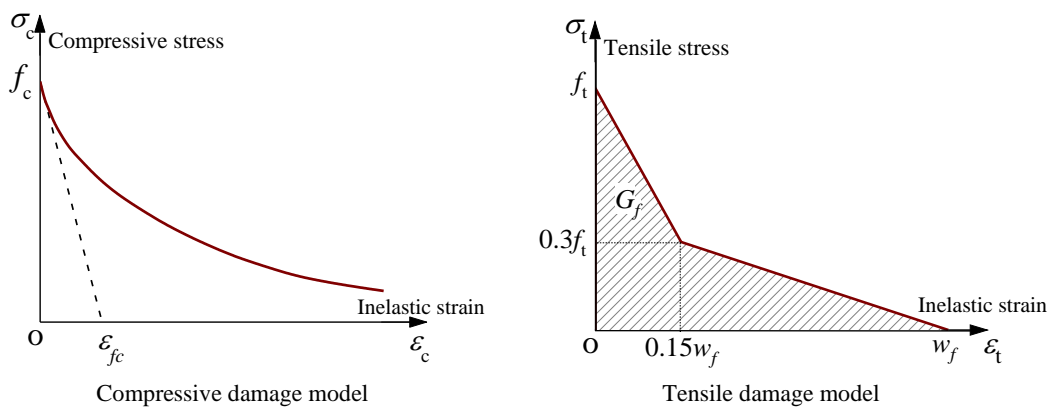


Fig. 3. Constitutive model of concrete [21]

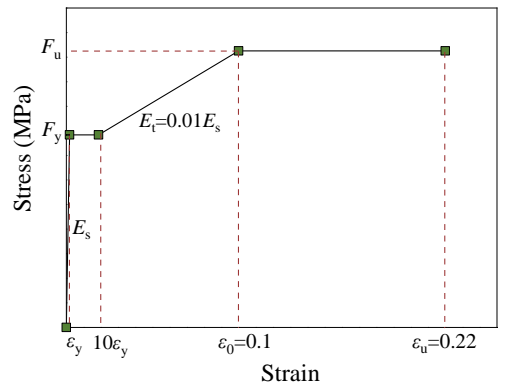


Fig. 4. Constitutive model used for steel tube and internal reinforcement

Three types of contact interface models were used in this study to model the different interfaces.

 The contact between the concrete fill and the steel tube was modeled with the "AUTOMATIC_SURFACE_TO_SURFACE" function, with a coefficient of friction of 0.35 [22]. This is a two-way treatment of contact; penetration of the follower node and the leader surface must be checked in both directions.

- 2. The contact between the concrete fill and internal steel reinforcing bar was modeled using the "BEAM_IN_SOLID" function, which invokes constraint-based (or penalty-based) coupling between the embedded reinforcing bars and the concrete fill.
- 3. The contact between the steel tube and the load cradle also was modeled with the "AUTOMATIC SURFACE TO SURFACE" function with a coefficient of friction of 0.6.

The endpoints of the support cradles were fixed translationally in all three directions (X, Y, and Z). These endpoints are free to rotate to simulate the support rotations.

The load cradles were translationally constrained in the longitudinal direction and rotationally constrained about the longitudinal and horizontal transverse to the plane of loading. All nodes of the concrete fill on both ends of the model of the specimen were constrained to the center node using the Nodal Rigid Body command. This constraint simplified the application of the axial load in the models that had an axial load and avoided stress concentrations in the concrete elements.

Table 2 presents the information for seven specimens that failed in a shear or flexure-shear mode. In this table, a is the length of the shear span [10]. The outer diameter (D) was the same for all specimens (20 in or 508 mm). The value of L_T is also given. Specimens 8 (reference specimen), 14, 15, and 20 were controlled by shear failure and therefore their shear strength was used to validate the shear strength predictions. Specimens 10, 13, and 16 were clearly influenced by the shear response but they also developed their flexural capacity and flexure influenced the response. The specimens varied in their (i) aspect ratio of the shear span, (ii) tail length, and (iii) concrete strength. The value of the varied parameter is highlighted in bold in Table 2.

The modeling approach was validated by comparing both the predicted response and the post-test damage [12]. The comparison of measured and predicted shear force-deflection behavior for each is provided in Table 2 and shown in Fig. 5.

The FEM provided an accurate prediction of the peak shear resistance and corresponding displacement, as shown in Fig. 5 and Table 2. The simulation results indicate the model captures the influence of the (i) aspect ratio, (ii) concrete strength, and (iii) tail length. These results are a significant improvement beyond prior FEM results [11,12]. This improvement is primarily a result of the accuracy of the concrete damage plasticity model in LS-Dyna.

The ability to account for the aspect ratio suggests that the model can account for the impact of changes in the shear span, which is critically important for piles in the soil as the aspect ratio of a portion of the pile can change with soil properties. The model is not sensitive to this change and therefore can capture the pile behavior in shear, flexure-shear, and flexure (the latter can be found in [10]). Here the focus is on shear and flexure-shear only so the models will use a small aspect ratio of 0.25, as recommended by Kenarangi and Bruneau [11].

The following discussion provides a focus on two selected specimens, one that failed in a shear mode (Specimen 14) and one that failed in a flexure-shear mode (Specimen 10). The selected specimens are highlighted in blue in Table 2. Note that Specimen 8 and Specimen 10 are similar except for the additional internal, longitudinal reinforcement. This reinforcement changes the failure mode to shear, suggesting that findings by Lehman et al. [10] are accurate, that is most of the CFSTs used in the field do not benefit from additional internal reinforcement unless it is required for the connection.

Comparing the simulated (dashed line) and the measured (solid line) results for Specimen 10 (as shown in Fig. 5a) demonstrates that this modeling approach provides an accurate assessment of the response to a vertical deflection of approximately 25 mm. This disparity is expected in most specimens, in particular shear-critical specimens. At larger deformations, there was an asymmetry in the experimental damage, resulting in larger shear and significantly larger shear deflection in one shear span. The simulation will not capture this asymmetry, since the damage in the FEM is symmetric unless an initial asymmetry is introduced into the model. However, even with this difference, the results are accurate. The tube tore at the bottom approximately 340 mm (15.5 in) south of mid-span after significant flexural and shear deformation occurred. The shear deformations and diagonal shear cracking and deformation were all particularly severe in the south shear span. The average ratio of the measured to predicted strengths was 0.99 of measured with a standard deviation of 0.05.

Table 2. Properties and FEM results for selected specimens used for validation

No	Damage Mode	a/D	a (mm)	F _y (MPa)	f' _c (MPa)	$arepsilon_y$	F _u (MPa)	L_T (mm)	$ ho_l$	V _{n-sim} (kN)	V_{n-exp} (kN)	$\frac{V_{n-sim}}{V_{n-exp}}$
8		0.375	190	372	45	0.00177	456	2D	2.0%	3709	3368	1.10
14	G1	0.25	127	382	59	0.00182	492	2 D	0	3501	3657	0.96
15	Shear	0.25	127	382	60	0.00182	492	5D/8	0	3791	3527	1.07
20		0.25	127	392	19	0.00187	458	2D	0	2934	3161	0.93
10		0.375	190	372	42	0.00177	456	2D	0	3072	2934	1.05
13	Flexure -shear	0.375	190	372	37	0.00177	456	D/2	0	2998	3160	0.95
16	Silvai	0.375	190	392	59	0.00187	458	2D	0	3322	3409	0.97

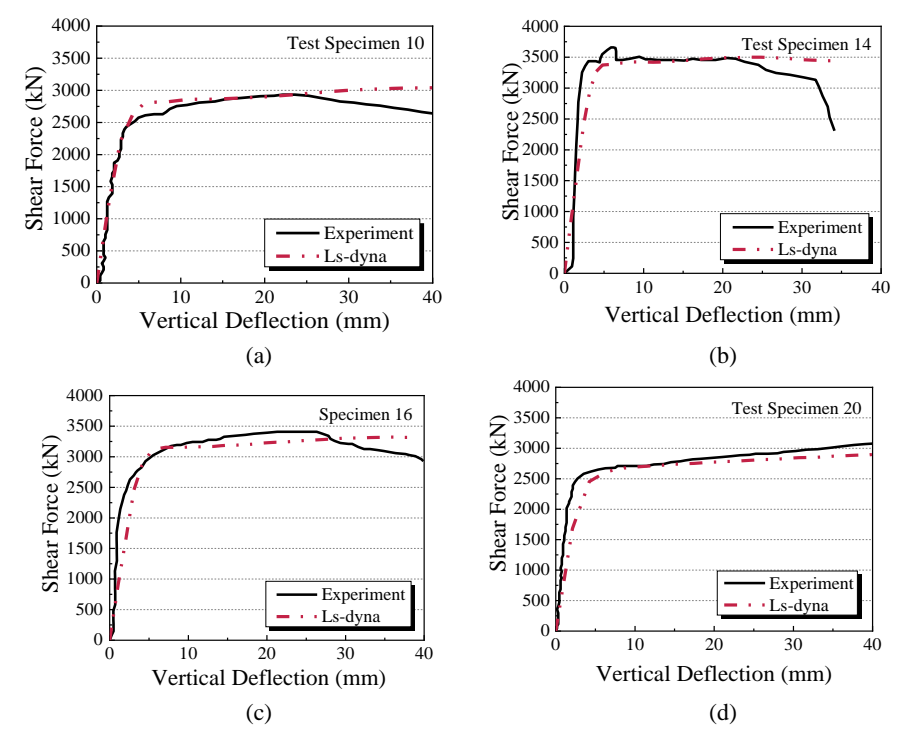


Fig. 5. Comparison of selected experimental and measured shear force-deflection behavior for four specimens failing in shear or flexural-shear: (a) Specimen 10, (b) Specimen 14, (c) Specimen 16, and (d) Specimen 20

Specimen 14 had a shorter shear span length and significant shear deformation. Fig. 5b indicates that the response is well captured until approximately 25mm of vertical deflection. This suggests that the model is accurate to this displacement level, and therefore the peak strength should not be assessed beyond this displacement level.

Fig. 6 compares the observed (photographed) damage and the simulated damage for the tube and the concrete fill for Specimen 14. This comparison was made for this specimen since the damage within the concrete fill was captured in the images in Fig. 6. The final state of the steel tube from the test and simulation was compared. The stress state of the steel tube is well captured. The entire circumference of the tube yields, as shown by parallelograms that were originally a rectangular grid on the tube. The minimum principal stress vectors and value of the tension damage parameter (indicated by the colors with red being fully cracked) characterize the condition of the concrete fill are shown in Fig. 6. Diagonal cracks in the concrete fill within the shear span were simulated by the FEM. Similar comparisons were noted for other specimens. Specimen 14 was adopted as the reference for the parametric study (Section 4).

The predicted response by the above FEM method also provides an understanding of the progression of yielding, cracking, and failure as well as the important damage and stress states for circular CFST responding in shear. The progression of these response modes is shown in Fig. 7 and outlined as follows:

- 1. At initial loading, diagonal strutting action is apparent in both shear spans.
- 2. As the shear force increases, the stress is distributed along the shear span; stress concentrations are not observed.
- 3. With an increase in the deformation demand, yielding initiates in the shear area and gradually distributes throughout the shear span.
- 4. After full yielding around the circumference of the tube, the stress in the steel tube approaches the ultimate strength.
- 5. The full circumference of the tube in the shear span reaches the ultimate strength.
- 6. Tearing of the tube initiates.
- 7. Tearing leads to fracture of the tube.
- 8. Finally, after tearing the tube and damage to the concrete, the CFST fails in shear. The steel tube is severely deformed but remains intact. As such, the tube can sustain stresses past strain-hardening and restrain separation of the concrete, which permits pronounced strength increase past yielding. This action allows the CFST to reach a shear strength that exceeds the tube alone. It is noted that all the failure of models was caused by the fracture of the steel tube, while the concrete was crushed at a very beginning deflection of the order of 2.5 mm. However, crushing of the concrete had little effect on the computed resistance, because the circular tube confined the crushed concrete, and the resistance was dominated by the behavior of the steel tube.

The separate force-deflection curves for concrete and steel contributions were calculated from the simulation and are shown in Fig. 7. In the figure, the contributions of steel and concrete are normalized by their respective lower bound shear strengths, i.e., shear strength of the steel tube before initial yielding and the lower bond strength of plain concrete. These are defined as the base strengths, V_c and V_{st} , which are defined in Eqs. (11) and (12), respectively. Note that the shear strength attributed to the concrete depends on the units of the concrete compressive strength, as shown in Eq. (11).

$$V_c = 0.167 \sqrt{f_c'} A_c \text{ (MPa)}, \quad 2 \sqrt{f_c'} A_c \text{ (psi)}, \quad 0.0632 \sqrt{f_c'} A_c \text{ (ksi)}$$
 (11)

$$V_{st} = 0.6F_{v}0.5A_{s} \tag{12}$$

The midspan deflection, Δ , is normalized by the length of the shear span, a, to define a normalized deflection.

exceed the yield stress)

Three zones of response are presented: (1) pre-yield, (2) post-yield and strain hardening, and (3) failure. Before yielding the steel tube, the shear resistance of the steel tube and concrete fill increases linearly with displacement. The peak resistance of the concrete fill corresponds to the yield point of the steel tube. At the initiation of yielding of the steel tube, the strains and deformation of the steel increase more rapidly, and the shear resistance of the steel increases, whereas the concrete contribution begins to degrade. This degradation associated with steel tube yielding is expected as the steel cannot yield without concrete damage. As the steel tube yields in shear, its effective stiffness decreases, and therefore cracks in the concrete open without resistance but do not fail since the tube remains intact. As such, the shear resistance of the concrete fill decreases in the post-yield and strain hardening zone, and the shear resistance of the steel tube increases. As the cracks continue to open in the concrete fill, the steel tube provides an increasingly larger portion of the shear resistance. Experimental results (Fig. 5) agree with the analyses shown here, and fracture occurs at an average normalized deflection of approximately 20% or larger [10]. The maximum shear resistance occurs shortly before the fracture of the steel tube, which causes failure of the CFST.

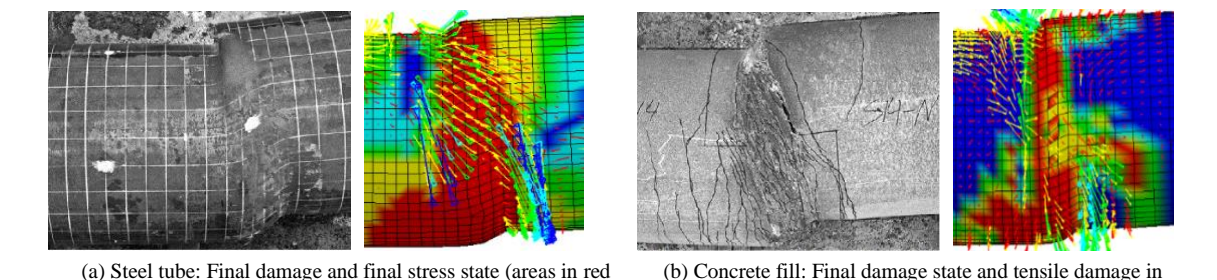


Fig. 6. Comparison between observed and simulated response of Specimen 14

the shear span

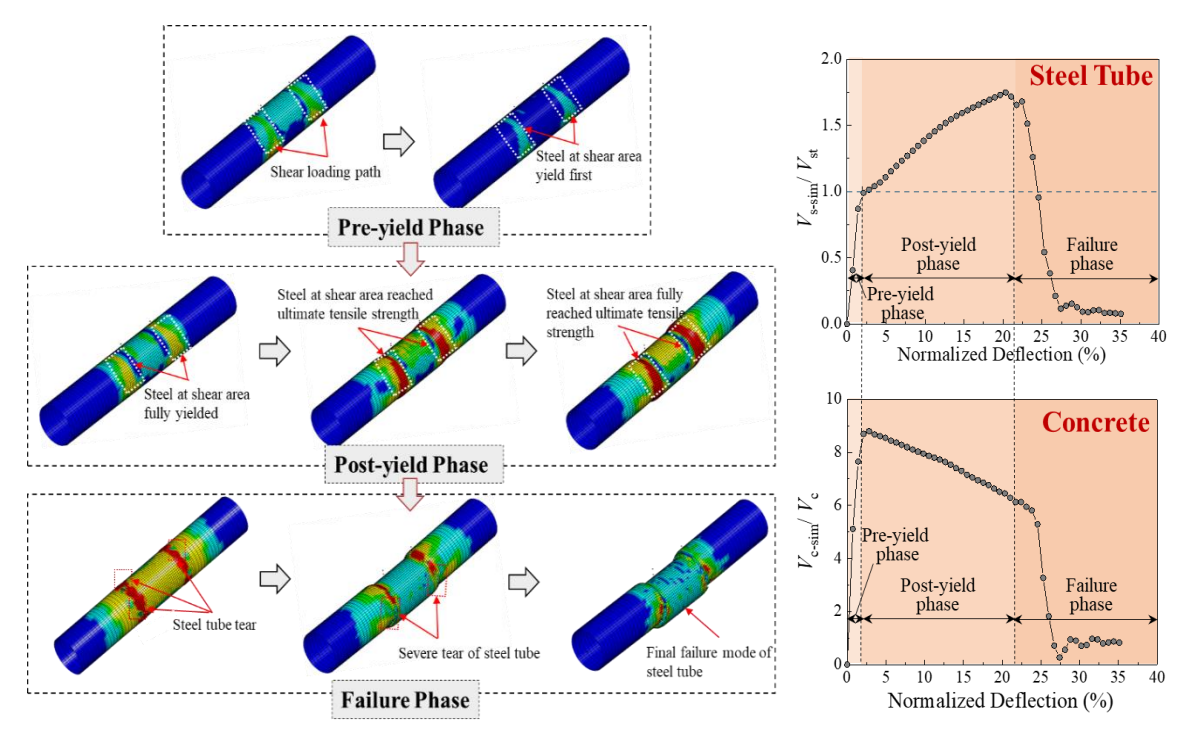


Fig. 7. Sequence of shear behavior for circular CFST

4. Parametric study

The results of the prior section demonstrate that the FEM is capable of (1) accurately simulating the shear strength, (2) accurately simulating the progression of damage, and (3) accurately simulating the failure mode. As such it was deemed appropriate to expand the experimental studies to investigate values of important but unstudied values of design parameters.

The specific parameters of the study and their values were as follows:

- 1. The stress-strain relationship of steel tube includes: (i) the yield stress (F_y) of 241, 392, and 483 MPa, (ii) ratio of tensile to yield (F_u/F_y) of 1.33, 1.43, 1.50, 1.53, and 1.77 and (iii) strain hardening ratio (E_t) of $0.004E_s$, $0.006E_s$, $0.007E_s$, $0.008E_s$ and $0.01E_s$.
- 2. Axial load ratio, P/P_0 : 0, 0.1, 0.2, 0.3, 0.4 and 0.5 where $P_0 = A_s f_y + A_b f_{yb} + 0.95 A_c f_c'$.
- 3. Tube diameter to wall thickness ratio, D/t: 40, 60, and 80.
- 4. Compressive strength of concrete fill, f_c' : 25, 50, and 70 MPa.
- 5. Internal reinforcement ratio, ρ_{int} : 0, 1.04, and 2.01%.
- Enhanced composite action through the inclusion of a supplemental steel rib on either side of the CFST.

The results were used to investigate the impact of each parameter to advance the understanding of how different parameters change the shear resistance of CFSTs. In addition to evaluating the trends in terms of the design parameters and the shear strength, these results were also used to quantify the shear strength contributed by the concrete fill and the steel tube, respectively.

As shown in Table 1, the US design equations underestimate the shear resistance achieved in experiments. These results will allow the development of more accurate design equations. The shear resistance of circular CFSTs is primarily provided by the steel tube and concrete fill and can be divided into these two contributions as

$$V_n = \alpha_c V_{ct} + \beta_c V_c \tag{13}$$

where V_n is the total shear resistance of CFST, α_c is the amplification coefficient on the base strength of the steel tube, and β_c is the amplification coefficient of the base contribution of concrete fill.

The following sections describe each design parameter varied in this study; for each design parameter, a series of values are investigated. The results of the models are then presented in terms of the total shear responses (V_n) , the contribution of steel (V_{st-sim}) and the contribution of concrete (V_{c-sim}) to evaluate the importance of the parameter. The contributions are calculated by LS-Dyna, which integrates the stresses around the cross-sectional areas of steel and concrete, to assess V_{st-sim} and V_{c-sim} , respectively. This is illustrated in Fig. 8. The cross-section at the midpoint of the shear region is used to determine each component, that is the component as in Fig. 8.

To investigate the contributions of the steel tube and concrete fill, the plots use normalized contributions of steel and concrete to elastic base strengths (V_{st} and V_c as defined in Eqs. 11 and 12) as well as the normalized deflection. In the following sections, the peak shear resistance and the corresponding contributions of each component were the computed shear resistance at 15% normalized vertical deflection, because this deformation level provides the best approximation of the peak strength for all tests and simulations.

4.1. Stress-strain relationship of steel tube

The stress-strain relationship of steel tubes is important to determine the shear resistance beyond initial yielding. Fig. 7 clearly shows that the shear resistance of a CFST is a function of the nonlinear response of the steel tube. As such, the effect of changes in the yield stress (F_v) , ultimate tensile-to-yield strength ratio

 (F_u/F_y) , and post-strain-hardening modulus (E_t) on the shear behavior of CFST was studied. The reference model is based on Specimen 14 and had a D/t ratio of 80 and $f_c' = 50$ MPa.

Fig. 9 shows the constitutive models. Three different yield stresses were studied: 241, 392, and 483 MPa with the same strength ratios and ultimate strains, specifically $F_u/F_y = 1.33$ and ε_0 of 0.1.

Fig. 10 shows the contributions of the steel tube and concrete fill in two different ways (this approach is also used for the other parameters). Fig. 10a shows the magnitude and percentage of each component to the total shear strength as a function of F_y . Fig. 10b shows the normalized force-deformation response of the steel tube; Fig. 10c shows the normalized force-deformation response of the concrete fill. The results indicate that the normalized shear strength contribution of the steel tube is independent of F_y , as expected. In contrast, the normalized shear strength contribution of the concrete fill increases modestly with F_y . This increase is likely a result of the confinement provided by the tube which increases with F_y .

The same approach is used to investigate the impact of strain hardening, expressed as the ratio of the ultimate to yield strengths (F_u/F_y) . The value of F_u/F_y depends on the steel grades. Steels with higher yield stress generally have smaller F_u/F_y ratios.

Fig. 11 shows the stress-strain curves used for this study. Each curve has the same F_y and E_{sh} , with different values of F_u/F_y , specifically 1.3, 1.5, and 1.8.

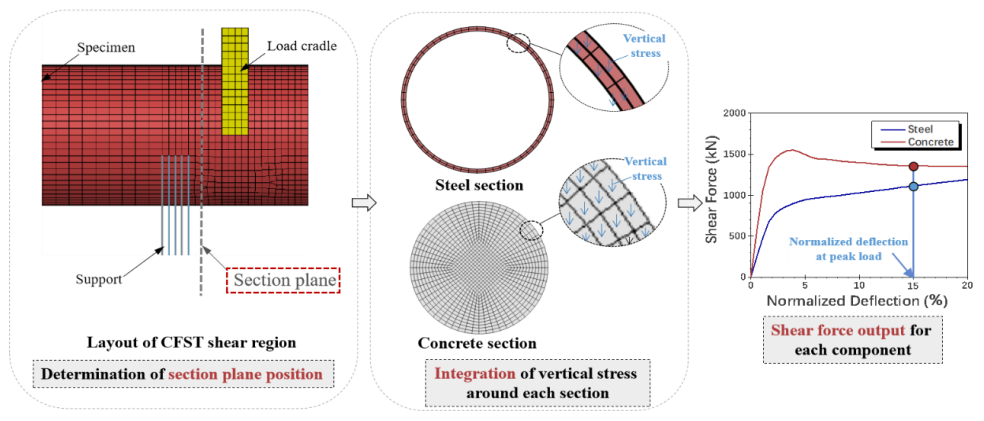


Fig. 8. Illustration of the calculation process for steel and concrete contribution

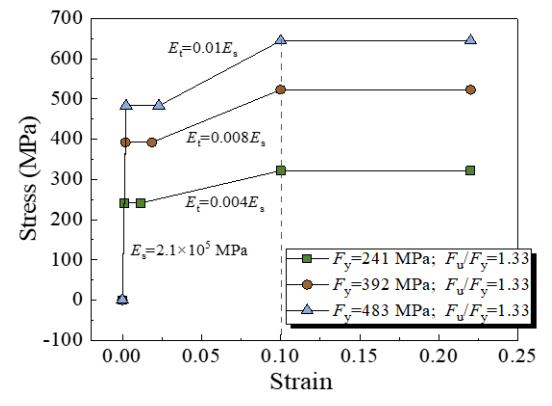
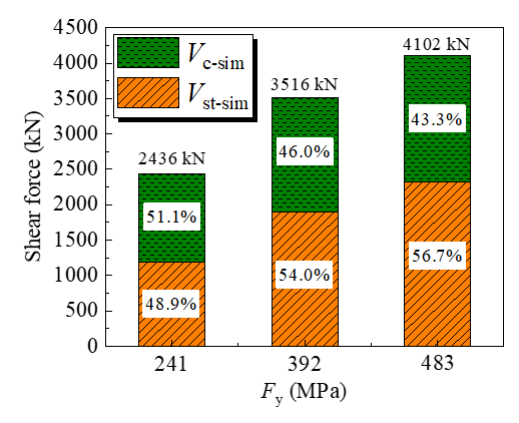


Fig. 9. Stress-strain model of steel tube



(a) Relative contributions of the components of the shear strength

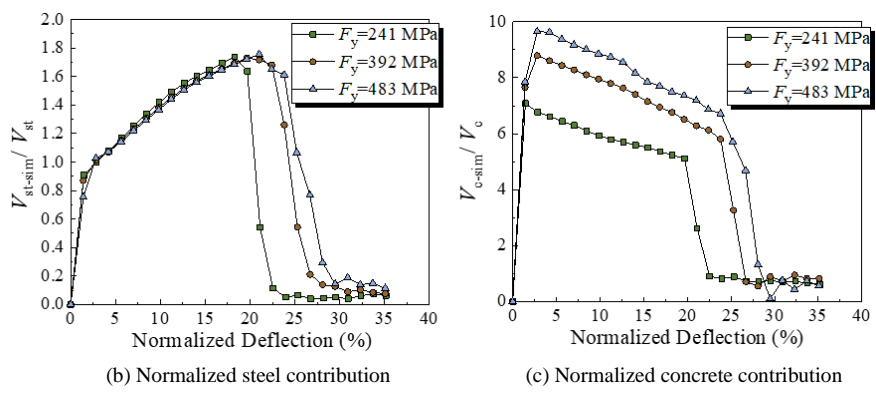


Fig. 10. Contributions of (a) steel tube and (b) concrete fill as a function of F_{ν}

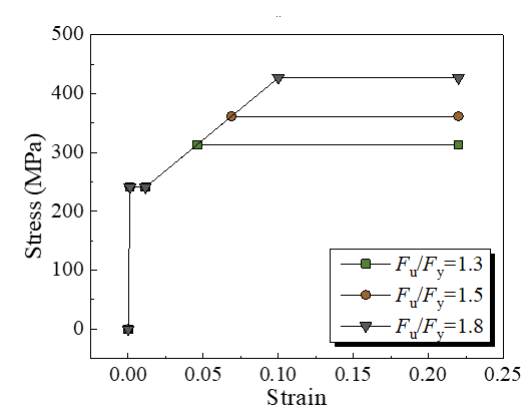


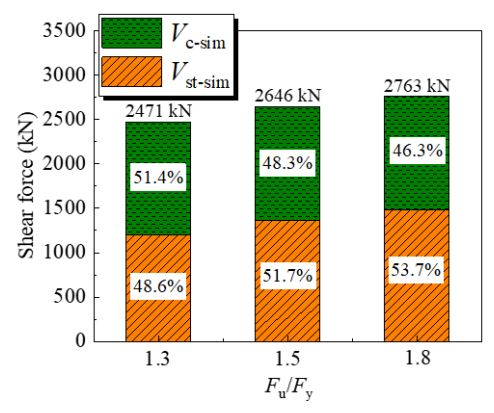
Fig. 11. Stress-strain model of steel tube

Fig. 12 shows the results using the same three plots described and shown in Fig. 10. Fig. 12a shows that an increase of F_u/F_y increases the shear strength. The contribution of the steel tube to the shear strength also increases with F_u/F_y , where the concrete contribution decreases with an increase in the F_u/F_y of the steel tube. This suggests that the F_u/F_y ratio is an important factor and should be included in the shear design equation.

The differences in the response curves occur after initial yielding (Fig. 12b). In Fig. 12b, the peak steel contribution increases with larger values of F_u/F_y . In contrast, the concrete contribution remains the same,

as shown in Fig. 12c. Most importantly, the normalized steel resistance increases with F_u/F_y suggesting that the shear contribution of the steel tube depends on F_u rather than F_y . (The values of F_u corresponding to the different F_u/F_y ratios of 1.3, 1.5, and 1.8 are 313.3, 361.5, and 426.9 MPa, respectively).

A third study was undertaken to investigate the impact of the steel material properties, specifically to investigate F_u alone. To retain the same value of F_y , E_t was varied to change F_u . Fig. 13 shows the stress-strain models used for these analyses. In contrast to Fig. 11, the value of F_u changes as a function of E_t rather than a prescribed stress ratio. The response of the models in Fig. 14 is similar to that shown in Fig. 12, where the increased strength is again largely a function of F_u and does not depend on the value of E_t . The concrete contribution is not influenced by the value of F_u .



(a) Relative contributions of the components of the shear strength

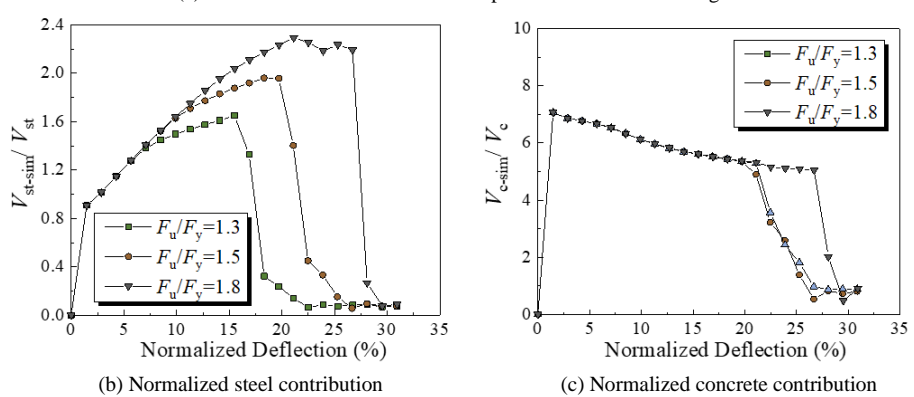


Fig. 12. Shear behavior of CFST with different F_u/F_v

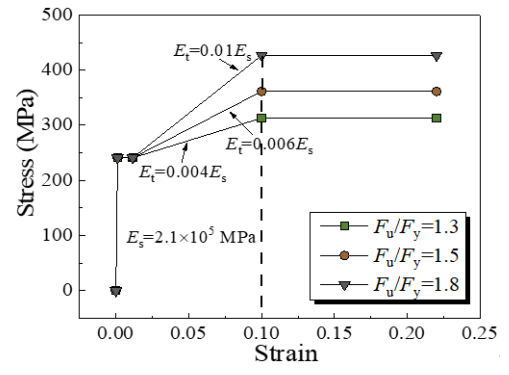


Fig. 13. Stress-strain model of steel tube

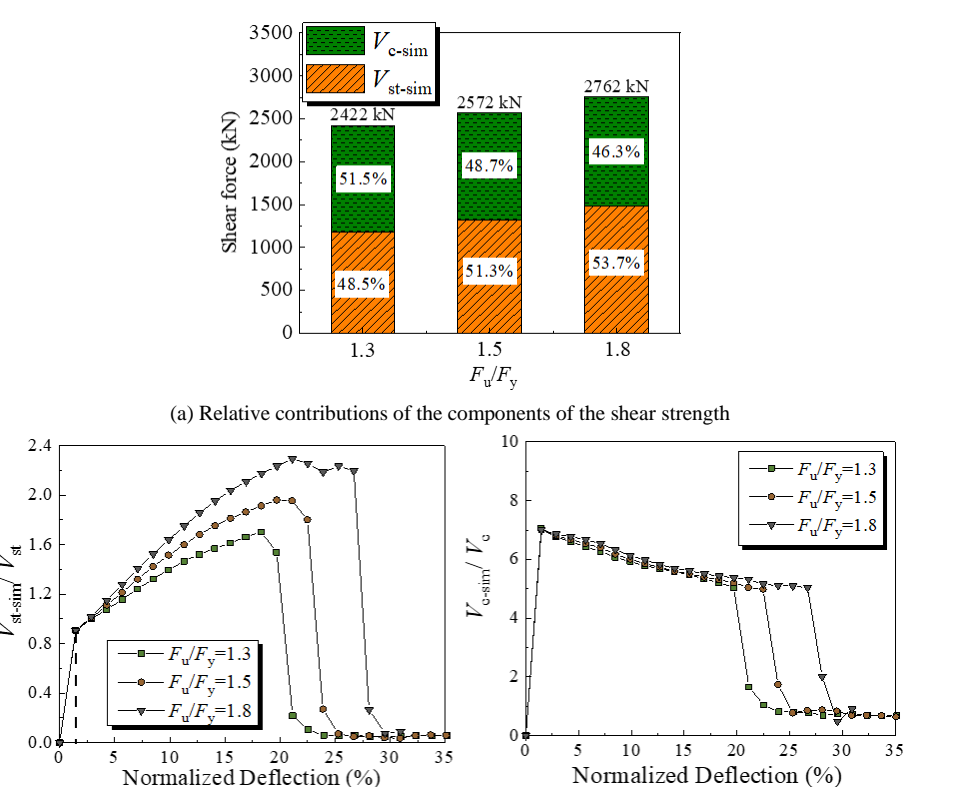


Fig. 14. Steel and concrete contributions as a function of F_u/F_v

(c) Normalized concrete contribution

(b) Normalized steel contribution

4.2. Axial load ratio

The shear strength of reinforced concrete columns is a function of the axial stress ratio [23]. This portion of the parametric study was undertaken to investigate the influence of the axial load on the composite member. To investigate the impact of the axial load on the total strength as well as the components of the shear capacity, a constant axial load was applied on the central nodal rigid body point of the ends of the model to the concrete fill alone. Recall, to all nodes in the cross-section on the end surface were constrained, as described previously. The following values of P/P_0 were studied: 0, 0.1, 0.2, 0.3, 0.4, and 0.5 with D/t = 80, a/D = 0.25, $f_c' = 50$ MPa and $F_v = 392$ MPa.

Fig. 15 shows the simulation results including peak strength as a function of P/P_0 (Fig. 15a), total shear-deflection response (Fig. 15b), the response of the steel tube (Fig. 15c), and the response of the concrete fill (Fig. 15d). As expected, the shear strength of the concrete contribution increases with an increase in the axial load ratio. Fig. 15a and b show that axial compression significantly increases the shear resistance of CFST, with a nearly linear relationship between V_n and P/P_0 . Fig. 15b shows the stiffness of the CFST is largely independent of the axial load ratio, however, the strength degrades at a smaller deflection with an increase in axial load ratio.

The individual contributions of the steel tube and concrete fill are shown in Figs. 15c and d, respectively. The contribution of the steel tube decreases slightly with an increased axial compressive load ratio for the model with a normalized axial stress ratio of 0.5; this reduction is expected as the steel tube must resist the normal stresses from the axial load which, in terms, reduces its shear capacity. This reduction of steel tube resistance is also shown in Fig. 15a. The contribution of concrete fill increases significantly with the increase

of axial compressive load ratio (Fig. 15a and d) because the concrete cracking is restrained by axial compression, this finding reflects the shear-strength equations for reinforced concrete columns (ACI 318-19 [23]). The slope of the post-peak degradation increases with a larger axial load ratio.

4.3. Diameter to thickness ratio

Three D/t values 40, 60, and 80 were investigated as shown in Fig. 16. The other key parameters were held constant; constant values of P/P_0 , a/D, f_c' and F_v were 0.2, 0.25, 50 MPa, and 392 MPa, respectively.

In ANSI/AISC 360, there are three compactness limits for CFST subject to flexural loading: (i) compact, (ii) non-compact, and (iii) maximum permitted. Other codes have similar limits. All use the ratio of $c_o E_s/f_y$ where c is the constant that varies with the compactness limits. The values of c_o are 0.15, 0.19, and 0.31 for compact, noncompact, and maximum limits, respectively. These models with $F_y = 50$ ksi meet the compactness limit; the models with higher steel strengths meet the non-compactness limit. In all cases, the response of the CFST in shear does not depend on D/t limits (compactness limit), although the AISC equation does require compact sections to get the full capacity of the shear strength attributed to the concrete.

Fig. 16a shows the peak concrete fill and steel tube contributions using a bar chart. The total height of each bar is the total shear strength of circular CFST; each bar indicates a different D/t ratio. The total shear strength reduces with an increase in D/t, as expected. This reduction is due to the reduction in the shear area of the steel tube.

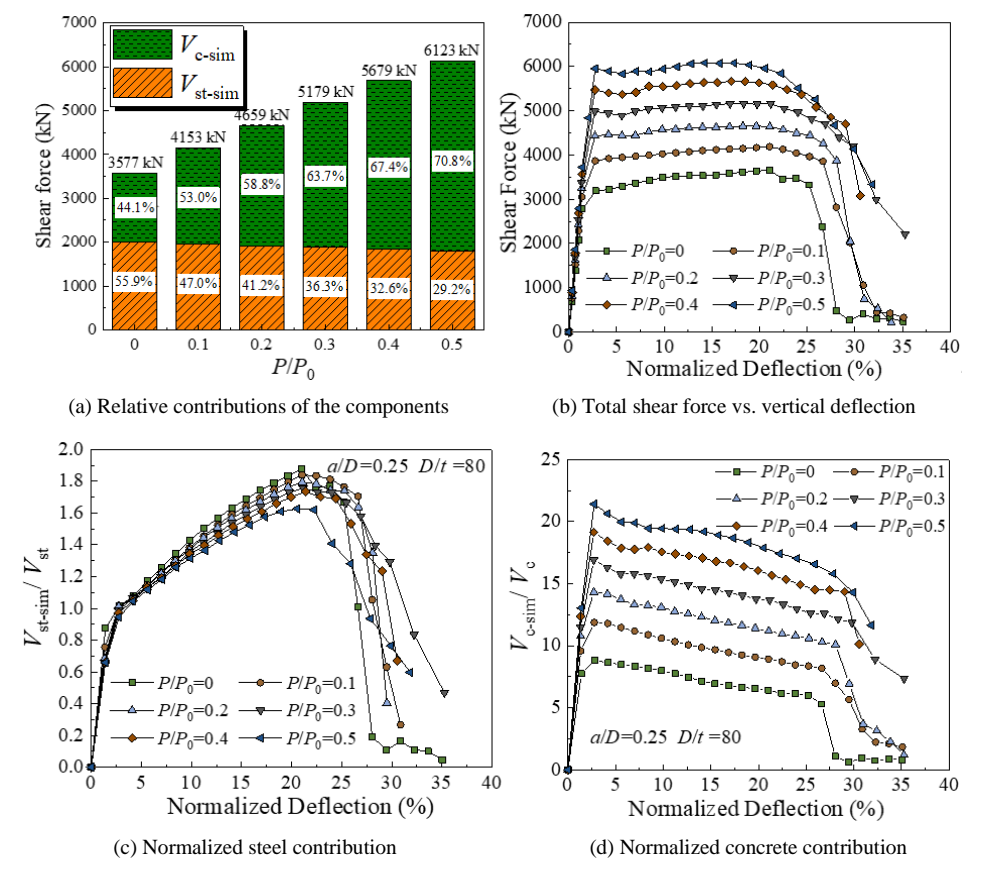
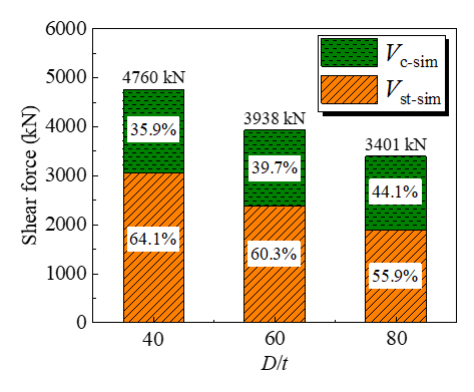


Fig. 15. Effect of axial load ratio on shear resistance (D/t = 80, a/D = 0.25, $f'_c = 50$ MPa, $F_y = 392$ MPa)



(a) Relative contributions of the components of the shear strength

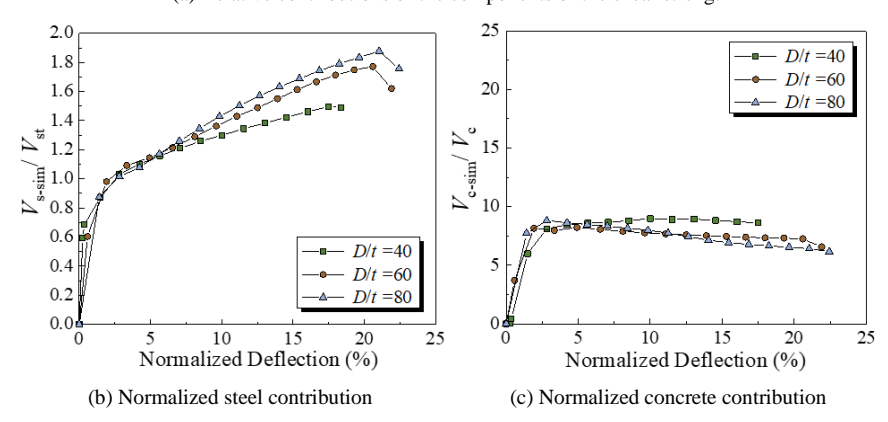


Fig. 16. Shear response with different D/t ratio $(P/P_0 = 0, a/D = 0.25, f'_c = 50 \text{ MPa}, F_y = 392 \text{ MPa})$

The normalized contributions of steel and concrete components are shown in Figs. 16b and c. The impact of the D/t ratio is not as significant when each contribution is normalized. At a normalized vertical deflection of 15%, the normalized steel component is smallest for the smallest D/t ratio of 40 and increases for D/t ratios of 60 and 80. In contrast, the smallest D/t ratio results in the highest normalized concrete contribution, although the increase is small and unlikely to be included in the design equation. The smaller D/t ratio provides a more stable response for the concrete. Because the steel tube contributes most of the shear resistance, the slight increase in the concrete resistance will not have a significant benefit to the shear capacity relative to F_u of the steel tube and does not need to be included in the design equation. In all cases, the D/t limit for non-compact sections provides similar normalized shear strengths, which suggests that the AISC equation should depend on the non-compactness limit of $0.19^{E/F_y}$, not the compactness limit of $0.15^{E/F_y}$.

4.4. Concrete strength

Three concrete compressive strengths were studied: 25, 50, and 70 MPa. Fig. 17a shows the peak shear strength of the two components and the total shear strength of the CFST for each value of f'_c . The shear contribution of the concrete fill increases with an increase in f'_c as expected. Fig.17b and c show the variation of the normalized contribution of steel tube and concrete fill with deflection. The analyses indicate that the normalized response does not depend on the concrete strength. This suggests that compressive strengths up to 70 MPa can be used in CFSTs.

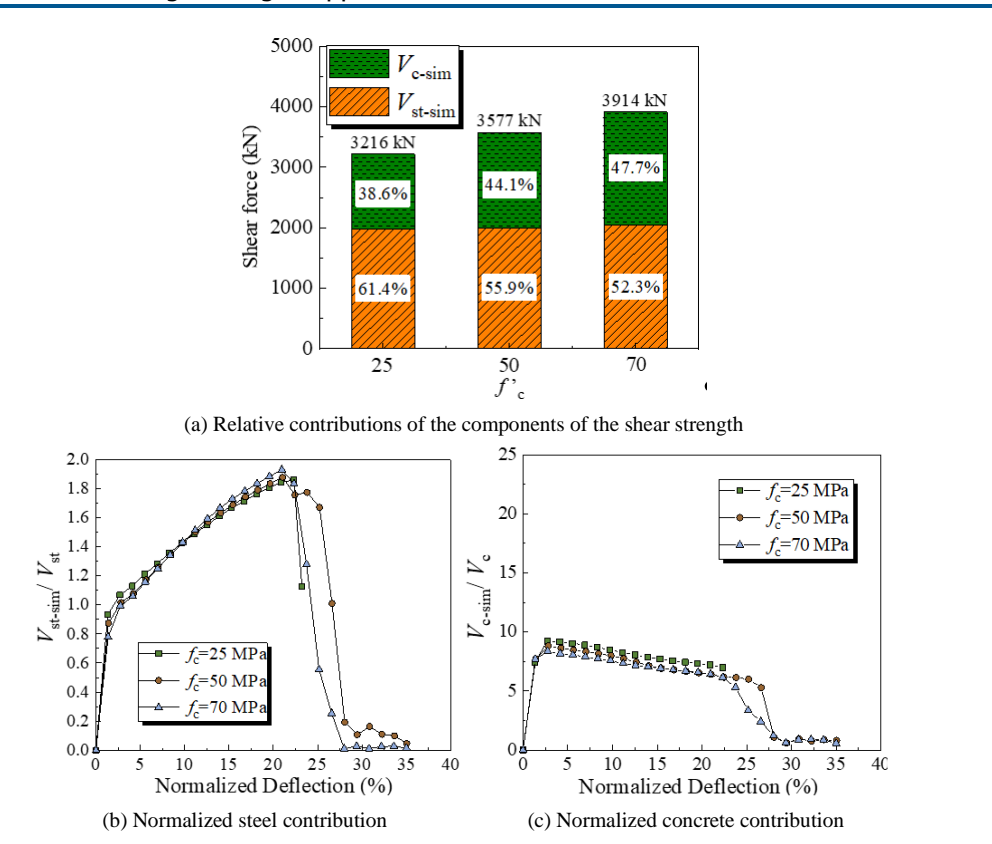


Fig. 17. Shear response with different concrete strengths $(D/t = 80, P/P_0 = 0, a/D = 0.25, F_v = 392 \text{ MPa})$

4.5. Internal reinforcement ratio

In some cases, CFSTs are reinforced with internal, longitudinal reinforcing bars. As discussed previously, internal reinforcement is not needed for most CFST components. The most common use of internal reinforcement is to connect the CFST to an adjacent concrete component. In addition, the internal reinforcement provides additional strength to enhance the steel tube in cases of fire protection or corrosion. In most cases, internal reinforcement along the entire tube length is not required.

Two values of longitudinal reinforcement ratios (ρ_{int}) were studied: approximately 1% and 2%. These models were compared to the reference CFST (D/t = 80, $P/P_0 = 0$, $F_y = 392$ MPa, $f_c' = 50$ MPa) with and without internal longitudinal reinforcement. Two different percentages were investigated: (i) 11 No. 5 bars or 1% and (ii) 11 No. 7 bars or 2%.

Fig. 18 shows the resulting response for these three models. Fig. 18a is a bar chart of the peak strengths for the three different internal reinforcement ratios (0%, 1%, and 2%). The shear strength attributed to the internal reinforcement is negligible relative to the steel tube and concrete fill. In addition, the increase in the shear resistance is not directly proportional to the internal reinforcement ratio. A CFST with a D/t of 80 has an equivalent reinforcement ratio of 5% reinforcing (due to the tube only). Adding 2.01% of internal reinforcement increases the area of the steel by approximately 40% but the increase in total shear resistance is only 33%. This is in general agreement with past experimental results and numerical simulations [10].

Fig.18b shows the shear response of internal reinforcement normalized by its axial yield capacity, or A_bF_{yb} . This figure shows that increasing ρ_{int} can lead to a slight reduction in the normalized reinforcement contribution, and the contribution to the shear capacity is negligible. Fig. 18c shows that internal reinforcement does not influence the contribution of steel tubes. Fig. 18d shows that internal reinforcement

increases the contribution of the concrete fill because the internal rebar restricts crack opening and propagation in the concrete fill, therefore increasing its resistance to shear.

4.6. Additional mechanical bond: Steel rib

Research indicates that the bond strength can impact the shear strength [10]. Research on the bond of CFSTs indicates that a single supplemental rib at the end of the tube is an effective mechanism to supplement the bond without damaging the concrete [24]. This was studied through a series of analyses where a supplemental steel rib, referred to herein as a rib, was added at the end of the model as shown in Fig.19. The inner and outside diameter of the steel rib were 473.5 mm and 495.3 mm, respectively. The length in the longitudinal direction is 50.8 mm. The ribs of steel were to be welded to the inside of the tube at the end of the concrete, as shown in Fig. 19 in the blue region. To simulate this connection, the ribs were modeled using constant-stress solid elements with rigid body constraints. This section compares the strength of paired models with and without the supplemental ribs.

The base model used the reference model characteristics: $F_y = 392$ MPa and D/t is 80. Fig. 20 compares the total shear strength of CFST for pair models with and without end ribs; for each pair of models, a single concrete strength was investigated. Comparing Figs.20a and b shows that the rib can enhance the shear resistance of CFST by increasing the shear resistance of the concrete fill, as shown in Figs. 20e and f. The rib is recommended to enhance for CFSTs where there is a concern about the bond capacity to achieve full composite action.

5. Evaluation of codified and proposed design expressions

The results from the parametric study and the prior experimental data were used to evaluate the current and propose a new expression to better predict the shear resistance of CFSTs.

Table 4 provides a comparison of the mean and (COV) (given in parenthesis) for the full dataset of experimental and simulation results from this parametric study that exhibited shear failure. Previous evaluations of the existing expressions in current codes [14–17] were not accurate when compared with the experimental results as previously shown in Table 1. Table 4 expands on the findings in Table 1, which provided the ratio of the simulated (experimental and numerical) strength to the codified expressions. In addition to comparing the full expression, the table also compares each component to the simulated component for the applicable expression (i.e., this comparison is only provided for expressions with multiple components). The table presents the averages and coefficient of variation (COV) for the ratio of the simulated results from each FEA model to the predictions by existing code expressions [14–17]. Most of the code expressions [14–17] severely underestimate the concrete and steel contributions to shear resistance; the expressions in Chinese code-1 overestimate the shear strength and thus are unsafe.

Evaluation of the experimental and simulated results suggests that the best form of the CFST shear strength expression is a two-component model, with the two components being the contribution of the concrete fill and the contribution of the steel tube. Basing the expression solely on one or the other will result in inaccuracies and underestimations, as indicated in Tables 1 and 4.

To investigate the accuracy of the most common core equation in the US from ANSI/AISC 360 (given by Eq. (1) where K depends on the compactness ratio, i.e., only members with tubes that meet the limit of $0.15E/F_y$ have a concrete contribution that exceeds $\sqrt{f_c'}$ with f_c' in psi, the salient AISC equations were selected and compared to FEM results, as shown in Fig. 21. As mentioned earlier, the AISC equations underestimate the shear strength, the concrete contribution, and the steel contribution. However, this underestimation is more severe for the concrete component. There are two reasons for this. First, important factors, such as F_u/F_y , P/P_0 and ρ_{int} , are not included in the equations. Second, the concrete contribution is

only fully realized for sections meeting the compactness limit. As a result, the equation underestimates the concrete contribution resulting in a high ratio of V_{n-sim}/V_{n-AISC} , which reduces the accuracy of AISC equations.

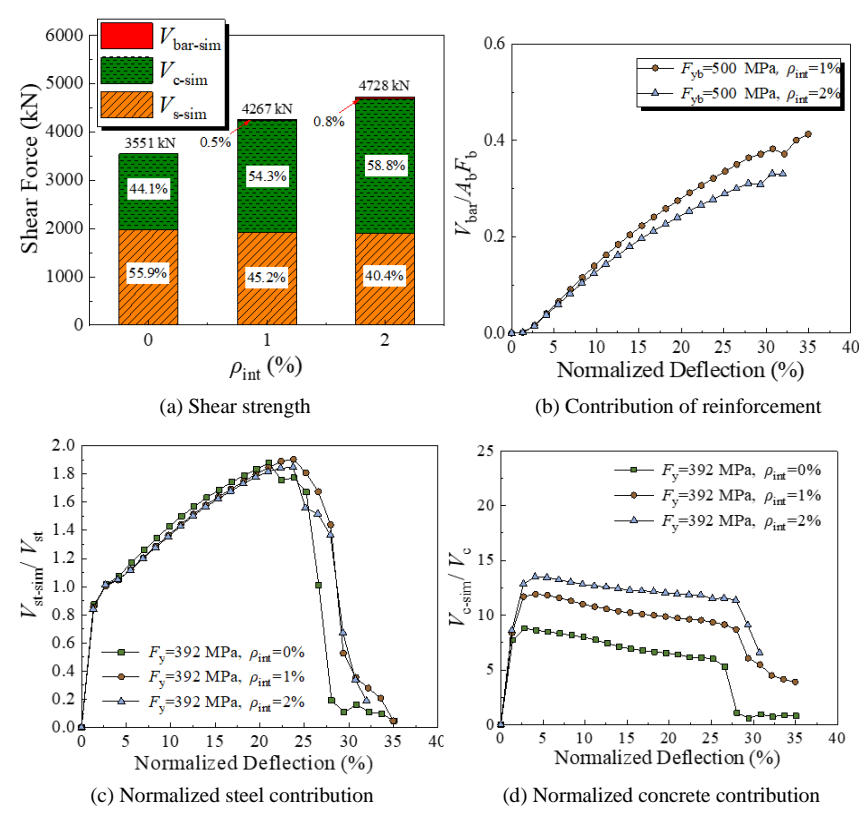


Fig. 18. Shear response with different internal reinforcement ratios (D/t = 80, $P/P_0 = 0$, $f_c' = 50$ MPa)

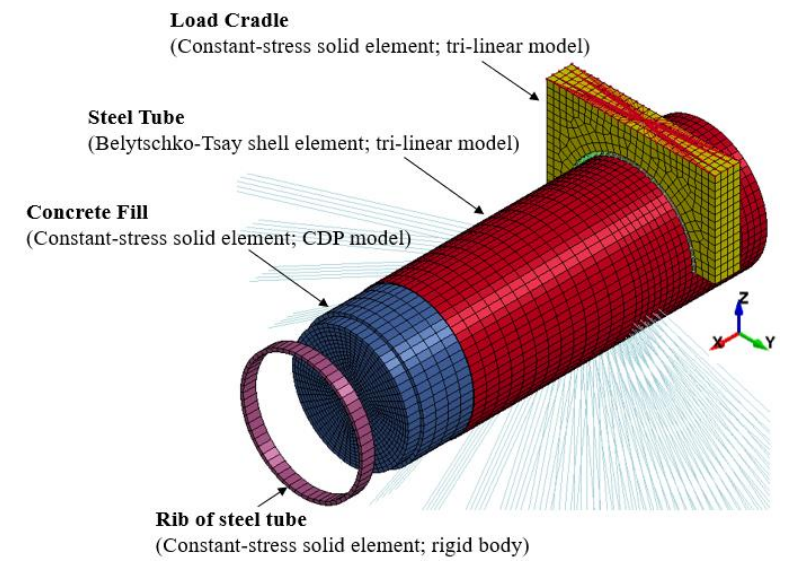


Fig. 19. Model of supplemental rib (only half of the model is shown)

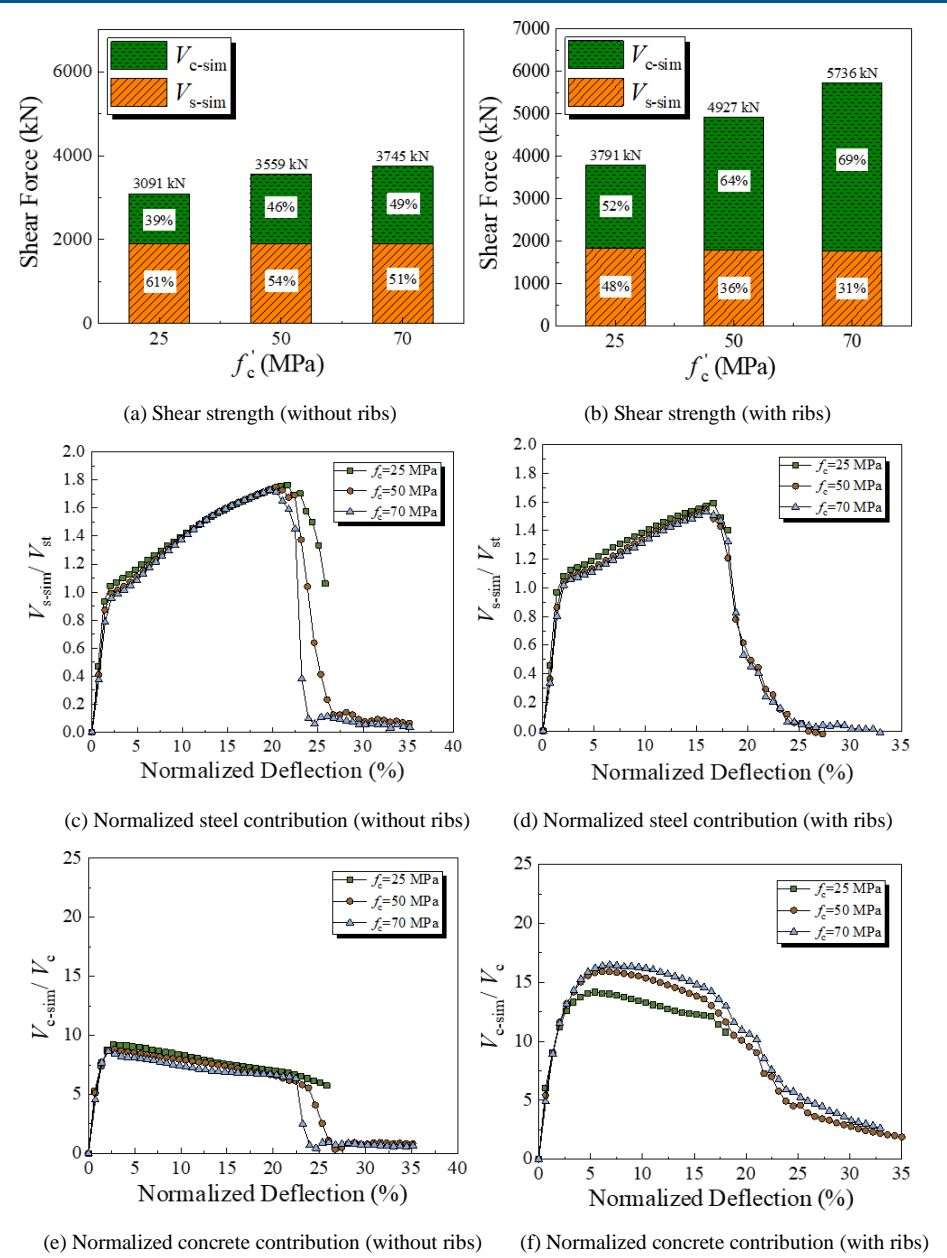


Fig. 20. Shear response of specimen with or without supplemental ribs

Table 4. Comparison of the concrete and steel contribution determined from FEA to codified equations

	AISC [14]	AASHTO [15]	Eurocode [16]	Chinese code 1 [17]	Chinese code 2 [17]
Concrete contribution	8.51 (0.55) ^a	3.56 (0.35)	_	_	1.68 (0.36)
Steel contribution	1.62 (0.075)	1.30 (0.078)	_	_	1.06 (0.080)
Total	2.71 (0.27)	1.94 (0.16)	2.81 (0.18)	0.94 (0.18)	1.29 (0.17)

^a The value in bracket is the coefficient of variation (COV) for the ratio of predictions by code expressions to the results of FEM.

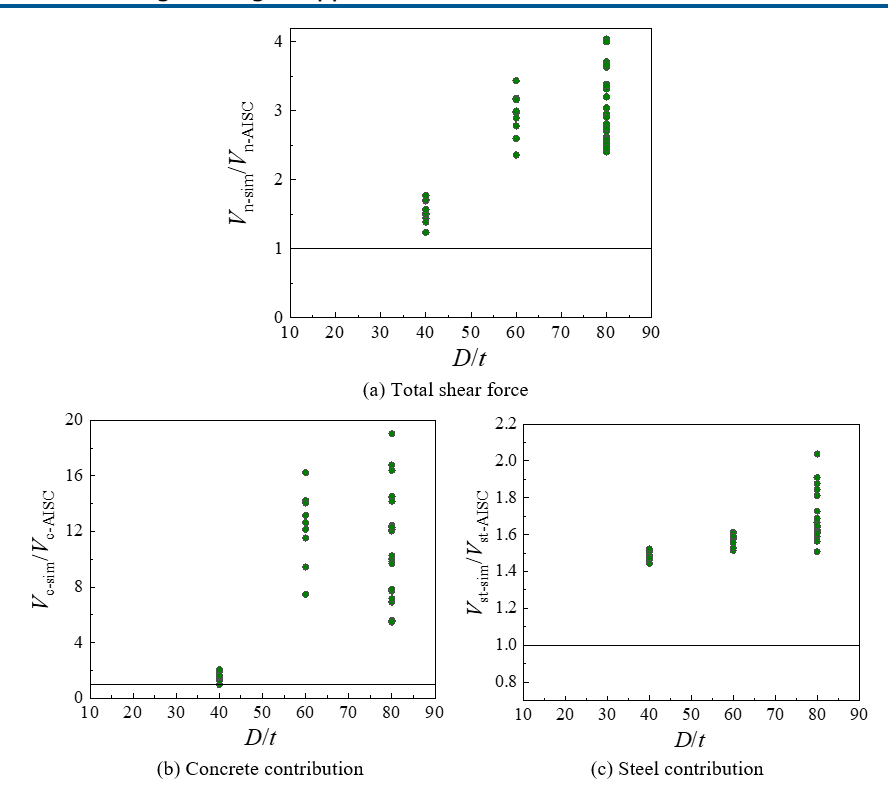


Fig. 21. Comparison of FEM results to predicted results by AISC equations

To improve the accuracy, four categories of parameters are included in a proposed equation: (1) normalized geometry (D/t), (2) material properties including concrete strength, yield strength, and the form of the stress-strain beyond yield, (3) axial load, and (4) internal reinforcement. To determine the values of the two contributing mechanisms, FEA is required for both experimental results and models of untested parameter values and untested parameters. The parameter studies show the following trends which should be included when developing a proposed design equation for the shear strength of CFSTs.

- The most important parameters were determined to be D/t, material strength including F_y , F_u and f_c' , and the axial load ratio. To a lesser extent, the internal longitudinal reinforcement also increases the contribution of concrete fill.
- An increase in F_u/F_y for a given value of F_y increases the shear strength contributed by the steel tube. This suggests that for a circular CFST, estimating the shear capacity of the tube using F_u might provide a more accurate estimate than using F_y alone.
- Small D/t ratios can result in a reduction in the contribution of the steel tube and a slight increase in the normalized contribution of the concrete fill because the steel tube with smaller D/t ratio does not yield fully around the section and therefore provides more constraint of and confinement to the concrete fill.
- The increase in axial load ratio and internal reinforcing ratio does not significantly impact the
 contribution of the steel tube to the shear resistance. Rather they increase the contribution of the
 concrete fill because both restrain crack opening and propagation.

These results suggest that the composite action in CFST, the enhancement of tube stiffness due to the restraint by concrete fill, and the strength of the concrete fill must be accounted for in the proposed design

expressions. Based on the prior observation and the regression analysis from the FEM results in this paper, the proposed design expressions are given as follows:

$$V_{n-vre} = \alpha_c V_{st} + \beta_c V_c \tag{14}$$

$$V_{st} = 0.6f_{\nu}(0.5A_s) \tag{15}$$

$$V_c = 0.167 A_c \sqrt{f_c'} \text{ with } f_c' \text{ in MPa}$$
 (16)

$$\alpha_{cc} = \frac{F_u}{F_v} \tag{17}$$

$$\beta_c = 7 + 20P/P_0 + 150\rho_{int} \tag{18}$$

The concrete contribution to the shear resistance includes the square root of the concrete strength (f_c) and the concrete shear area. In addition, the tests and simulation data show that an increase in P/P_0 and ρ_{int} increase the concrete contribution ($\beta_c V_c$) to the CFST shear resistance. An increase in F_y and a decrease in D/t decreases the concrete contribution to the total shear resistance. However, the influence of F_y and D/t is not as important as P/P_0 and ρ_{int} , which appears to be the key variable and should be included in the modifier on β_c . The expression in Eq. 18 is proposed for β_c . The expression was developed by using regression analysis to best predict the contribution of concrete fill while assuring a statistically conservative prediction.

Fig. 22 compares the components of the proposed design expression to the computed component contributions to the simulated resistance from the FEA. Fig. 22a shows the proposed shear contribution of the steel tube computed from the proposed design expression providing an accurate but slightly conservative estimate of the FEA results; the difference is within $\pm 15\%$. Similarly, the proposed shear resistance of concrete provides a conservative estimate of the FEA results; the majority of the results fit within $\pm 20\%$ (a few points are more conservative) as shown in Fig. 22b. This expression provides a more accurate, yet conservative, estimate of the concrete contribution and the steel contribution. (Note that experimental results cannot be used to evaluate the components since it is difficult to separate the measured strength into the two components and therefore the test data cannot be used for this evaluation.)

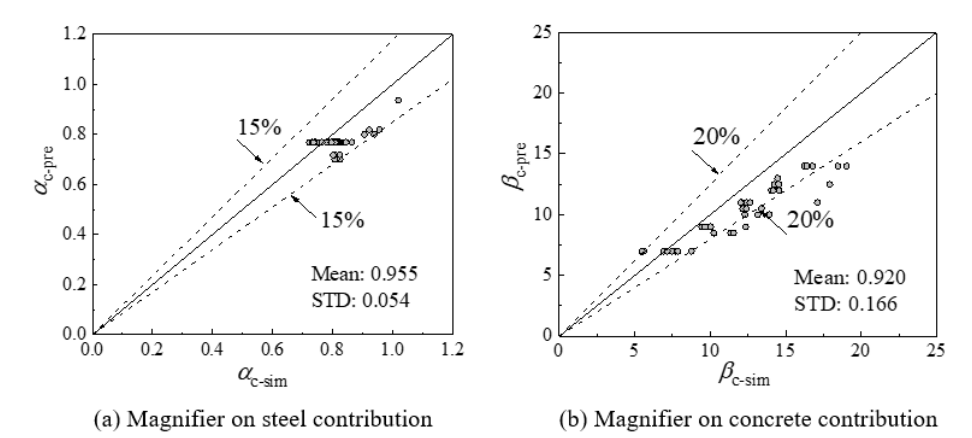


Fig. 22. Comparison of predicted component contributions using design expression to FEM results

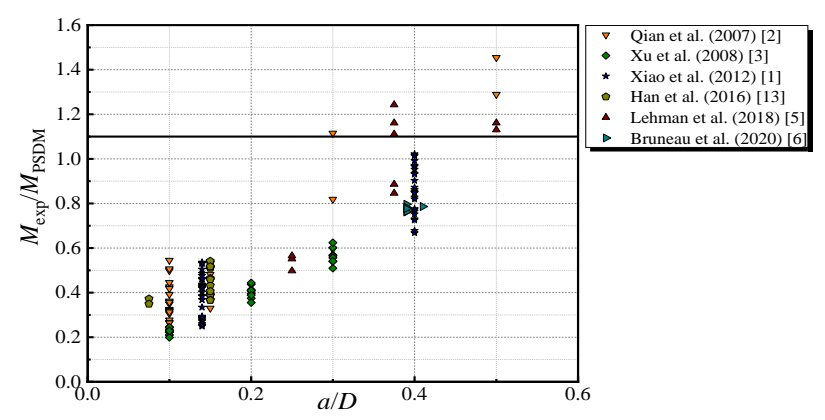


Fig. 23. Measured flexural strength (M_{exp}) to plastic moment capacity (M_{PSDM})

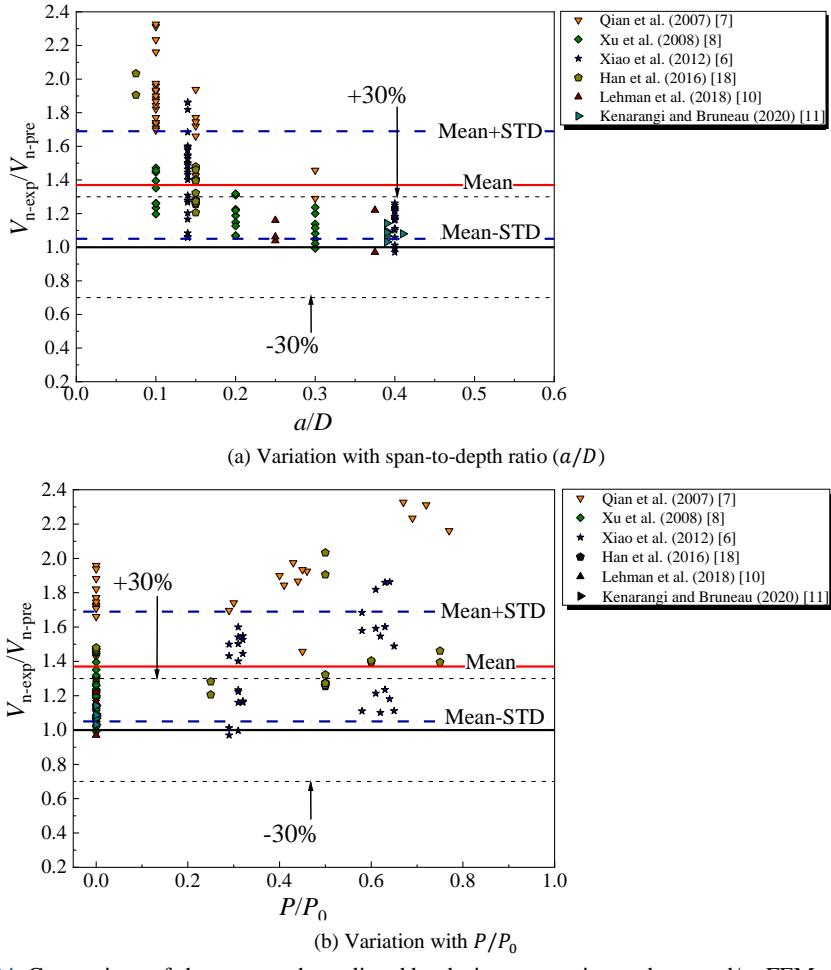


Fig. 24. Comparison of shear strength predicted by design expression and test and/or FEM results

The predicted results (V_{n-pre}) are compared with prior test results which failed in a shear-dominated mode. Before this comparison, the measured flexural strength (M_{exp}) for the available specimens was compared to the plastic moment capacity (M_{PSDM}) , which was determined by the plastic stress distribution

method, as shown in Fig. 23. The figure shows that some individual specimens by Qian et al. [7] and Lehman et al. [10] fail in flexure where $M_{exp} > 1.1 M_{PSDM}$; as such, these results are not included the following validation.

The evaluation of the components and V_{n-pre} are shown in Fig. 24. Fig. 24a shows the ratio of test results to predicted shear strength (V_{n-exp}/V_{n-pre}) as a function of shear span-to-depth ratio (a/D). The results conservatively predict test data $(V_{n-exp}/V_{n-pre}) > 1$ for 97% of the data) with an average ratio of 1.37. Fig. 24b compares the predictions to experimental results as a function of the axial load ratio (P/P_0) . This figure shows that the proposed equations are accurate for lower axial load ratios and give a conservative estimate of the shear strength for $P/P_0 \ge 0.4$.

The design expressions are valid for the following design parameter values: a/D of 0.075–0.5, D/t of 26–80, F_y between 241 MPa and 542 MPa, f_c between 19 MPa and 70 MPa, ρ_{int} ranging from 0% to 2.2% and P/P_0 between 0 and 0.77. The AISC resistance factor is retained as 0.85 resulting in a representative safety index β of 3.0 [25,26].

6. Summary and conclusions

The shear resistance of concrete-filled tubes has historically been either a function of the steel tube alone or the concrete fill alone. Newer approaches, such as AISC 360-22, use a two-component shear strength model. However, the components of the model can only be evaluated using results from validated finite element modeling since experimental work does not allow the separation of the two components.

This research project evaluated the shear resistance of CFST using advanced and verified modeling methods in the LS-Dyna software program. There are three phases of behavior, which were observed in the analyses and test results. The steel tube and concrete fill contribution increased rapidly in the elastic phase with relatively small strains. In the post-yield phase, the shear force in the steel tube increases while the concrete fill deteriorates. Ultimate failure occurs after significant inelastic shear strain and loss of shear resistance occurred with cracking, tearing, and fracture of the steel tube.

A parametric study was used to extend the experimental results. The combined database of simulated and experimental results was used to evaluate existing equations and provide the foundation for a newly proposed equation. The proposed equation was compared to the finite element results to assess the accuracy of the individual components as well as the total shear resistance. The proposed equation provides an accurate and slightly conservative estimate and is a large improvement over the current codified expression.

The parametric study results indicate the influence of specific design parameters on each component of the model. Specifically:

- The tensile strength ratio (F_u/F_y) of steel tube had a significant influence on the steel contribution and CFST shear resistance. The contribution of concrete fill was not affected by F_u/F_y .
- The shear resistance of the concrete fill increased linearly with the increase of axial load ratio when P/P_0 is less than 0.5. P/P_0 does not have a large impact on the contribution of the steel tube.
- The contribution of steel tube does not depend on the D/t ratio in elastic stage of behavior. At small D/t ratios, the shear strength of the concrete increases, and the member shear strength approaches the strength of the steel tube alone. This suggests that the designer need not meet the compactness limit; the non-compact limit provides a reasonable limit.
- CFST specimens with supplemental ribs have increased shear resistance because the rib restrains
 the slip of the concrete relative to the steel tube and cracking of concrete fill. The rib is needed in
 cases of shrinkage as well as straight seam tubes subjected to high flexural demands.

The most important result is the newly proposed design expression for shear resistance of circular concrete filled tubes. The comparison between the predicted and available test results shows that proposed

Strain at the failure of steel tube

 ε_u

equations can safely evaluate all experimental data with a mean experimental-to-predicted shear strength (V_{n-exp}/V_{n-pre}) ratio of 1.37 and a standard deviation of 0.32. This variation is significantly lower than those of current code equations in the US The resistance factor for the proposed design equations is 0.85 with the representative safety index of 3.0.

Appendix

Nomenclature

Nomenclatu	re
а	Shear span defined as the length between the maximum and zero moments
A_{s}	Cross-sectional area of steel tube
A_c	Cross-sectional area of infill concrete
A_{b}	Cross-sectional area of internal reinforcement
A_{sc}	Total cross-sectional area of CFST
D	External diameter of steel tube
$E_{\scriptscriptstyle S}$	Young's modulus of steel tube
E_{sh}	Modulus in the strain hardening region for steel tube
E_t	Tangent modulus of post-yielded region
$F_{\mathcal{Y}}$	Yield strength of steel tube
$\vec{F_u}$	Ultimate tensile strength of steel tube
F_{yb}	Yield strength of internal reinforcement
f_c'	Design value of concrete compressive strength
f_{sv}	Design value of circular CFST shear strength (add in equation number)
f_t	Uniaxial tensile strength of concrete
G_f	Fracture energy of concrete in tension
K_c	Coefficient in shear-strength equation in AISC/AISI 360. $K_c = 1$ for members with shear span-to-depth
C	(a/D) greater than or equal to 0.7, $K_c = 10$ for members with rectangular cross section and a/D less
	than 0.5
L	Length of CFST component
L_T	Tail (overhang) length of CFST test specimen beyond the support
M_{exp}	Measured flexural strength of circular CFST
M_{PSDM}	Plastic moment capacity
P	Axial load
P_0	Squash load $(A_s F_y + A_c f_c')$
V_0	Pure shear capacity of circular CFST
V_n	Total shear resistance of CFST
V_{n-sim}	Predicted shear strength of circular CFSTs by finite element model
V_{n-pre}	Predicted shear strength of circular CFSTs by proposed design equation
V_{n-exp}	Experimentally measured shear strength of circular CFSTs
V_{n-AISC}	Predicted shear strength of circular CFSTs by AISC equation
V_{st}	Base contribution of steel tube to shear strength of CFST
V_c	Base contribution of infill concrete to shear strength of CFST without coefficient
V_{st-sim}	Predicted steel shear contribution from finite element model
V_{c-sim}	Prediction concrete shear contribution from finite element model
$V_{st-AISC}$	Predicted steel shear contribution of circular CFSTs by AISC equation
V_{c-AISC}	Predicted concrete shear contribution of circular CFSTs by AISC equation
α_c	Amplification coefficient on the base strength of steel tube for circular CFST
α_{c-pre}	The value of α_c predicted by proposed design equations
α_{c-sim}	The value of α_c predicted by finite element model
$lpha_{sc}$	Ratio of area of steel tube to infill concrete area
$arepsilon_y$	Yield strain of steel tube
eta_c	Amplification coefficient of the base contribution of concrete fill for circular CFST
eta_{c-pre}	The value of β_c predicted by proposed design equations
β_{c-sim}	The value of β_c predicted by finite element model
$arepsilon_0$	Strain at the ultimate stress of steel tube

- The compressive damage parameter $\frac{\varepsilon_{fc}}{\Xi}$
- Constraint coefficient

Acknowledgments

The research work in this paper was supported by the Natural Science Foundation of Shaanxi Province of China (2021JM-367). Analyses were conducted using the Texas Advanced Computing Center (TACC). The authors acknowledge the Texas Advanced Computing Center (TACC) at The University of Texas at Austin for providing High-Performance Computing resources that have contributed to the research results reported within this paper. URL: http://www.tacc.utexas.edu

Conflict of interests

The author(s) declared no potential conflicts of interest with respect to the research, authorship, and/or publication of this article.

Funding

This research received no external funding.

Data availability statement

No new data were created or analyzed in this study.

References

- [1] Zhou H, Han HH (2019) Modelling the behaviour of concrete-encased concrete-filled steel tube (CFST) columns subjected to full-range fire. Engineering Structures 183:265-280.
- Wang FC, Xie WQ, Li B, Han LH (2022) Experimental study and design of bond behavior in concrete-filled steel tubes (CFST). Engineering Structures 268:114750.
- Subedi N, Thusoo S, Obara T, Kono S, Kaneko O, Hayakawa T, Watanabe H, Mukai T (2022) Flexural performance of cast-in-place concrete-filled steel tube piles under varying axial load. Thin-Walled Structures 174:109130.
- [4] Ran YH, Wang XL, Zhu YP (2022) Experimental and numerical study on dynamic response of concrete filled steel tubular pile subjected to oblique impact. Structures 39:917-927.
- Han X, Han B, Xie HB, Yan WT, Yu JP, He YK, Yan LB (222) Seismic stability analysis of the large-span concrete-filled steel tube arch bridge considering the long-term effects. Engineering Structures 268:114744.
- Xiao C, Cai S, Chen T, Xu C (2012) Experimental study on shear capacity of circular concrete filled steel tubes. Steel and Composite. Structures 13(5):437–449.
- Qian J, Cui Y, Fang X (2007). Shear strength tests of concrete filled steel tube columns. China Civil Engineering Journal 40(5):1-9.
- Xu C, Haixiao L, Chengkui H (2009) Experimental study on shear resistance of self-stressing concrete filled circular steel tubes. Journal of Constructional Steel Research 65(4):801-807.
- [9] Nakahara H, Tokuda S (2012). Shearing behavior of CFST short columns, In: Proceedings of 10th International Confenerence on Advances in Steel Concrete Composite and Hybrid Structures, Singapore, pp. 362–369.
- [10] Lehman D, Roeder C, Heid A, Maki T, Khaleghi B (2018) Shear response of concrete filled tubes part i: experiments. Journal of Constructional Steel Research 150:528-540.
- [11] Kenarangi H, Bruneau M (2020) Shear strength of composite circular reinforced concrete-filled steel tubes. Journal of Structural Engineering 146(1):04019180.
- [12] Lehman D, Roeder C, Heid A, Yoo JH (2018) Shear response of concrete filled tubes Part II: Analytical study. Journal of Constructional Steel Research 153(1):169–178.

- [13] Zhao MZ, Lehman DE, Roeder CW (2021) Modeling recommendation for RC and CFST sections in LS-Dyna including bond slip. Engineering Structures 229:111612.
- [14] American Institute of Steel Construction (2022) Specification for Structural Steel Buildings, Chicago, IL.
- [15] American Association of State Highway and Transportation Officials (2016) AASHTO LRFD Bridge Design Specifications. Washington, DC (7th with 2016 interims edition).
- [16] European Committee for Standardization (2004) BS EN 1994, Eurocode 4: Design of Composite Steel and Concrete Structures—Part 1-1: General Rules and Rules for Buildings.
- [17] GB 50936-2014 (2014), Technical Code for Concrete Filled Steel Tubular Structures. Ministry of Construction of The People's Republic of China, Beijing, China. China Architecture & Building Press (in Chinese).
- [18] Ye Y, Han LH, Tao Z, Guo SL (2016) Experimental behaviour of concrete-filled steel tubular members under lateral shear loads. Journal of Constructional Steel Research 122:226–237.
- [19] LSTC (2019) Keyword User's Manual, Volume II. Livermore, CA, USA: Version 11 R11.0.0.
- [20] Grassl P, Jirasek M (2006) Damage-plastic model for concrete failure. International Journal of Solids and Structures 43:7166–7196.
- [21] Grassl P, Xenos, Uystrom U, Rempling R, Gylltoft K (2013) CDPM2: A damage-plasticity approach to modeling the failure of concreteInternational Journal of Solids and Structures 50(24):3805–3816.
- [22] Moon JH, Lehman DE, Roeder CW, Lee HE (2013) Evaluation of embedded concrete-filled tube (CFST) column-to-foundation connections. Engineering Structures 56:22–35.
- [23] American Concrete Institute (2014) Building Code Requirements for Structural Concrete (ACI 318-19) and Commentary, Farmington Hill, MI.
- [24] Lindsley S (2021) Inelastic Behavior of Direct RC Column to CFST Pile Connections. MS Thesis, University of Washington.
- [25] Ravindra MK, Galambos TV (1978) Load and resistance factor design for steel. Journal of Structural Engineering Divizion, ASCE, 104 (ST9):1337–1353.
- [26] Galambos TV (1981) Load and resistance factor design. Engineering Journal/American Institute of Steel Construction 18(3):74–82.